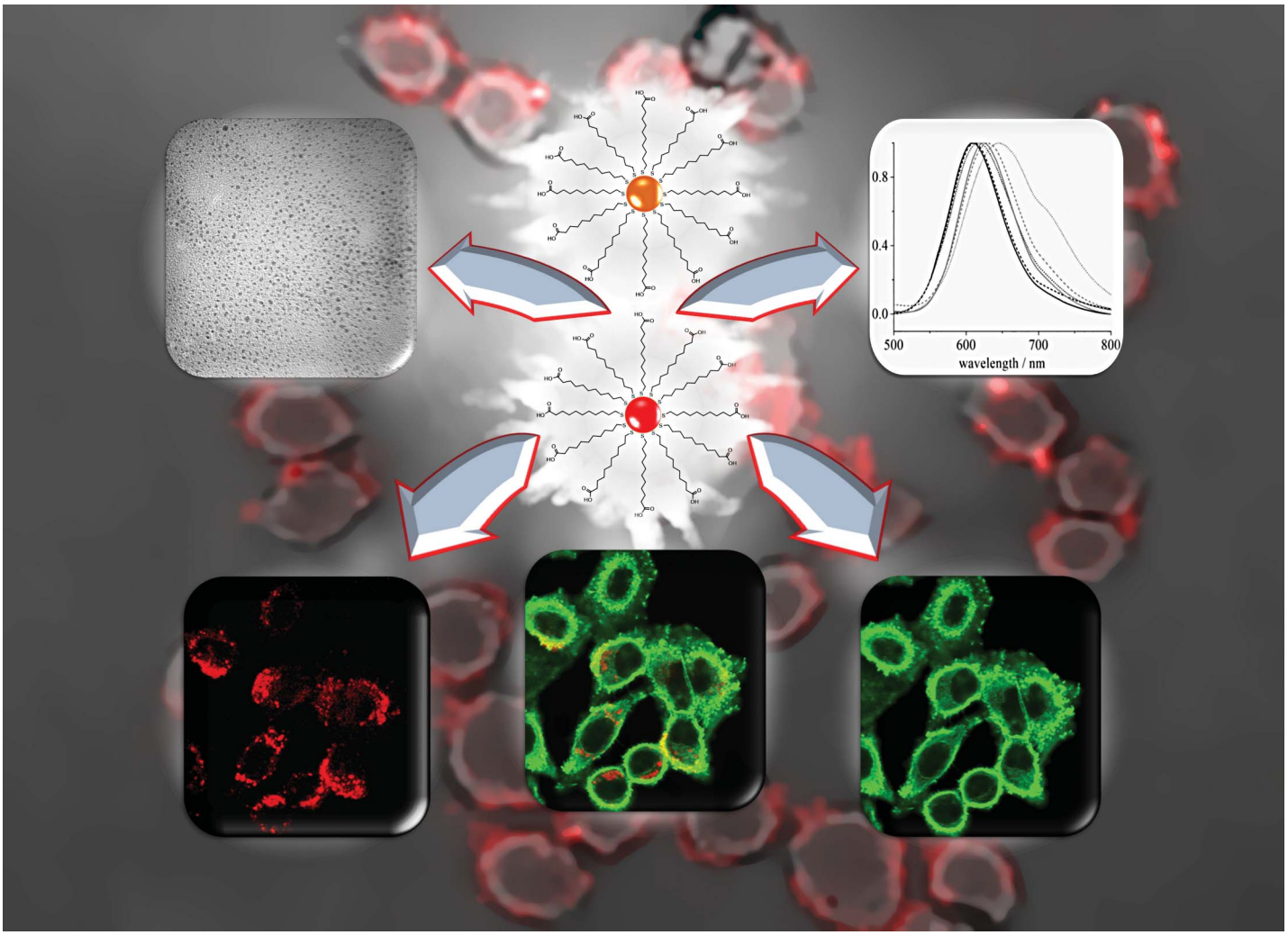

Highlighting research from the group of Prof. Matthias Epple at the University of Duisburg-Essen, Germany.

Title: An easy synthesis of autofluorescent alloyed silver–gold nanoparticles

Ultra-small silver–gold nanoparticles that can enter cells and be detected due to their autofluorescence have been synthesised and characterised.

As featured in:

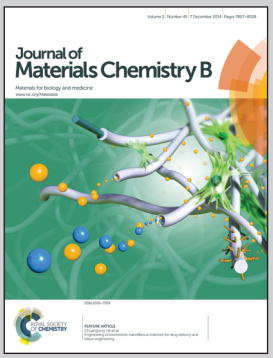

See Matthias Epple *et al.*, *J. Mater. Chem. B*, 2014, **2**, 7887.

ROYAL SOCIETY OF CHEMISTRY

www.rsc.org/MaterialsB

Registered charity number: 207890

Journal of Materials Chemistry B

PAPER

View Article Online
View Journal | View Issue

Cite this: J. Mater. Chem. B, 2014, 2, 7887

An easy synthesis of autofluorescent alloyed silver–gold nanoparticles

Simon Ristig, Diana Kozlova, Wolfgang Meyer-Zaika and Matthias Epple*

A one-pot synthesis of fluorescent bimetallic silver–gold nanoparticles in aqueous medium is presented. Carboxylic acid-functionalized nanoparticles were prepared with different metal compositions from 90 : 10 to 10 : 90 (*n* : *n*) for silver : gold with a diameter of 1.8 ± 0.4 nm. Pure silver and gold nanoparticles were prepared for comparison. Spectroscopic analyses showed that the ligand, *i.e.* 11-mercaptoundecanoic acid, binds to the particle surface by the thiol group, leaving the carboxylic acid accessible for further functionalization, *e.g.* by suitable coupling reactions. Nanoparticles with a silver content up to 60 : 40 showed autofluorescence with a large Stokes shift of about 250–300 nm (maximum wavelength of the emission between 608 nm and 645 nm). The intracellular localization of bimetallic silver–gold nanoparticles was studied in HeLa cells by confocal laser scanning microscopy (CLSM). The alloyed silver–gold nanoparticles showed no significant cytotoxicity at a metal concentration of 5 μg mL^{-1} for 24 h, but were cytotoxic to some degree at 50 μg mL^{-1} at higher silver content.

Received 19th June 2014
Accepted 17th September 2014

DOI: 10.1039/c4tb01010h

www.rsc.org/MaterialsB

Introduction

Metal nanoparticles have been the subject of many studies due to their distinct chemical and physical properties.[1–3] Especially gold and silver nanoparticles have been investigated to large extent, mainly due to their applications as antibacterial agents (silver) in imaging, drug delivery and tumour therapy (gold).[4–13] Recently, ultra-small noble metal nanoparticles (diameters of two nanometres and below), also denoted as clusters, have gained special interest.[14–18] With their size comparable to the Fermi wavelength, these ultra-small nanoparticles show molecular-like properties, for example autofluorescence, making them highly useful in analytical science, cellular and biological imaging.[2,19–22] There are numerous synthetic routes to prepare ultra-small gold nanoparticles, many of them utilizing the aurophilicity of thiol groups to achieve efficient capping in combination with strongly reducing agents to generate cluster-like gold nanoparticles.[14,23–26] Recently, ultra-small silver nanoparticles exhibiting autofluorescence have been prepared with methods and ligands as in the synthesis of gold clusters.[18,27–30] Frequently used capping agents are on the one hand proteins (*e.g.* BSA),[16,31–33] dendrimers[15,24] and polymers,[15,16] due to their excellent stabilizing effects. On the other hand, bifunctional organic thiols are prominent as they open up the possibility for further covalent functionalization of the nanoparticle system.[16,29,34] For instance, 11-mercaptoundecanoic acid (11-MUA) has been used in the synthesis of ultra-small gold and silver nanoparticles.[25,35,36]

Bimetallic nanoparticles of silver and gold are readily available in different sizes and compositions due to their similar lattice constants that make mixed crystals over the whole concentration range possible.[37–39] The generation of bimetallic clusters of silver and gold is a promising way to bypass the generally weak fluorescence intensity of gold clusters in comparison with other common fluorophores because the bimetallic clusters show a distinctly increased fluorescence quantum yield.[40,41] However, only a very few syntheses for ultra-small bimetallic silver–gold nanoparticles have been reported so far. Ganguly *et al.* synthesized fluorescent silver clusters on a micrometer-sized gold core and observed a synergetic effect between the two noble metals.[42] Udayabhaskararao *et al.* prepared fluorescent alloyed silver–gold clusters by core etching of silver nanoparticles with mercaptosuccinic acid, followed by a galvanic exchange reaction with gold.[43] Le Guével *et al.* synthesized fluorescent bimetallic silver–gold nanoparticles by co-reduction of silver and gold salts in the presence of glutathione.[40] Grade *et al.* prepared bimetallic silver–gold nanoparticles with a diameter of about 4 nm by laser ablation.[44]

Here we present the synthesis of ultra-small silver–gold nanoparticles with variable composition over the whole concentration range (from silver : gold 90 : 10 to 10 : 90) and the investigation of their fluorescent properties. The particles were prepared by co-reduction of silver and gold ions with sodium borohydride in water and simultaneous capping with 11-MUA. As the composition will influence the biological properties, we also studied the effect on HeLa cells.

Inorganic Chemistry and Centre for Nanointegration Duisburg-Essen (CeNIDE), University of Duisburg-Essen, Universitaetsstr. 5-7, 45117 Essen, Germany. E-mail: matthias.epple@uni-due.de

Experimental

Synthesis of nanoparticles

Prior to use, all glassware was cleaned with boiling *aqua regia*. The nanoparticles were synthesized by reduction with sodium borohydride in water in accordance with previously described procedures[25] with slight modifications: 500 μL of a solution of $HAuCl_4$ and $AgNO_3$ with a total metal content (Au + Ag) of 5 μmol, the ratio depending on the intended composition of the nanoparticles in terms of the weight of gold and silver, was added to 50 mL degassed ultrapure water under an argon atmosphere and light exclusion. For instance, for a composition of silver : gold 90 : 10, we used 4.5 μmol Ag and 0.5 μmol Au corresponding to 0.485 mg Ag and 0.098 mg Au, and corresponding to 0.764 mg $AgNO_3$ and 0.170 mg $HAuCl_4$. Then, 1 mL of a solution of 11-mercaptoundecanoic acid in ethanol (25 mM) and 1 mL of an aqueous solution of sodium hydroxide solution (50 mM) were added. After stirring the mixture for 10 min, 200 μL of a solution of sodium borohydride in water (200 mM; 0 °C) were added dropwise. The mixture was stirred for 10 min. For purification, the nanoparticles were precipitated by adding 25 mL ethanol. The particles were separated from unreacted gold ions and 11-MUA by centrifugation (3000 rpm, 10 min) and redispersed in ultrapure water. The precipitation and centrifugation were repeated twice. Finally, the nanoparticles were redispersed in 5 mL sodium borate/hydrochloric acid buffer (20 mM tetraborate, pH = 9).

Silver nitrate was obtained from Roth (p.a.), and $HAuCl_4$ was prepared by dissolution of gold in *aqua regia* according to standard procedures. Ultrapure water (Purelab ultra instrument from ELGA) was used for all preparation processes.

Characterization techniques

Transmission electron microscopy (TEM) images were taken with a Philips CM 200 FE. The dispersions were diluted with double-distilled water, drop-cast onto a carbon-coated copper grid and dried under ambient conditions. To estimate the particle size, 100 particles per image were manually measured and a histogram was compiled.

Differential centrifugal sedimentation (DCS) was performed with a CPS Instruments Disc Centrifuge DC 24000 (24 000 rpm, 28 978 g). As a density gradient, two sucrose solutions (8 wt% and 24 wt%) were used and capped with 0.5 mL dodecane as the stabilizing agent. The calibration standard was a poly(vinyl chloride) (PVC) latex in water with a particle size of 476 nm provided by CPS instruments. Calibration was carried out prior to each run. A sample volume of 100 μL was used.

Fourier transform infrared spectroscopy (FTIR) was carried out with a Bruker Alpha-Platinum FTIR with an attenuated total reflection (ATR) sampler. Prior to the measurements the samples were lyophilized with a Christ Alpha 2-4 LSC instrument.

Ultraviolet-visible spectroscopy (UV-vis) was performed with a Varian Cary 300 instrument. Suprasil® microcuvettes with a sample volume of 700 μL were used.

^{1}H-NMR-spectroscopy was carried out with a Bruker DPX 300 instrument. The spectra were recorded with 128 scans in $CDCl_3$ or D_2O with NaOD.

Fluorescence spectroscopy was performed with an Agilent Cary Eclipse spectrophotometer. Suprasil® cuvettes with a sample volume of 3.5 mL were used.

Atomic absorption spectroscopy was carried out with a Thermo Electron M-Series spectrometer with a graphite tube furnace after dissolving the particles in *aqua regia*.

Confocal laser scanning microscopy was performed with Leica TCS SP5 instrument using a 63×/NA 1.2 water objective. Alloyed silver–gold nanoparticle fluorescence was excited at 405 nm; the emission was recorded through a 635 nm long-pass filter. The immunofluorescence of actin staining was excited at 488 nm.

Cell experiments

For the cytotoxicity assay, HeLa cells were cultured in DMEM medium, supplemented with 10% fetal bovine serum (FBS), 100 U mL^{-1} penicillin, and 100 U mL^{-1} streptomycin at 37 °C in a humidified atmosphere with 5% CO_2. For the 3-(4,5-dimethylthiazol-2-yl)-2,5-diphenyltetrazolium bromide (MTT) cytotoxicity assay of alloyed silver–gold nanoparticles, the cells were trypsinized and seeded in 24-well plates with a density of 2.5×10^4 cells per well. After overnight cultivation the cells were incubated with different concentrations of bimetallic nanoparticles (5 and 50 μg mL^{-1}) in cell culture medium for 24 h and 72 h. The total volume of sterile ultrapure water for the MTT assay was normalized per each well. After incubation for 24 h or 72 h, the nanoparticle-treated cells were washed twice with cell culture medium and then incubated with 300 μL of the MTT solution (1 mg mL^{-1}) for 1 h at 37 °C under 5% CO_2 in a humidified atmosphere. Then the MTT solution was replaced with 300 μL DMSO. After 30 min, a 100 μL aliquot was taken for spectrophotometric analysis with a Multiscan FC instrument (Thermo Fisher scientific, Vantaa, Finland) at $\lambda = 570$ nm. The absorption of incubated cells was normalized to that of control (untreated) cells, thereby indicating the relative level of cell viability.

For uptake studies, HeLa cells were cultured in DMEM medium, supplemented with 10% fetal bovine serum (FBS), 100 U mL^{-1} penicillin, and 100 U mL^{-1} streptomycin at 37 °C in a humidified atmosphere with 5% CO_2. 12 h prior to the uptake experiments, the cells were trypsinized and seeded in cell culture dishes with 1×10^5 cells per well in 0.5 mL cell culture medium. For the uptake studies, the cells were incubated with 50 μg mL^{-1} Ag : Au 30 : 70 or Ag : Au 50 : 50 nanoparticles in serum-free medium for 5 h or in medium with 10% FBS for 5 h and 24 h. After selected times, cells were washed five times with PBS to remove adhering nanoparticles, fixed with 4% aqueous formalin for 20 min at room temperature. For immunofluorescence staining, the cells were incubated with Alexa-488-conjugated phalloidin (Invitrogen, Germany). Finally, the cells were studied by confocal laser scanning microscopy (Leica TCS SP5) using a 63×/NA 1.2 water objective.

Results and discussion

The morphology and size of the nanoparticles were investigated by transmission electron microscopy (TEM) and differential centrifugal sedimentation (DCS). Fig. 1 shows representative TEM images of two samples: Ag : Au 30 : 70 nanoparticles with an average diameter of 1.9 nm and Ag : Au 80 : 20 nanoparticles with an average diameter of 2.1 nm. TEM images showed that the nanoparticles were monodisperse and almost spherical, independent of their composition. The particles did not show signs of agglomeration. The average diameter as calculated from TEM images was between 1.8 nm and 2.1 nm. Although nanoparticles with a higher gold content appeared to be slightly smaller, the particles can be regarded as uniformly sized, independent of the ratio of silver to gold.

Disc centrifugal sedimentation (DCS) supported these findings, giving average particle diameters between 1.7 nm and 2.1 nm. It is noteworthy that the sizes derived from DCS were slightly smaller than those derived from TEM. As the density of the nanoparticles is a fixed parameter in DCS runs (which we had set to the weighed density of silver and gold, using the nanoparticle composition), the smaller size is a result of the shell of the organic ligand which lowers the effective density of the whole particle and slows down the sedimentation. DCS data were collected from 150 nm to 1 nm. We obtained narrow size distributions, indicating that the nanoparticles were monodisperse and stable against agglomeration (Table 1). No larger particles were observed by DCS. Fig. 2 shows a representative DCS size distribution of particles with the composition of Ag : Au 10 : 90. Dynamic light scattering was not possible due to the small particle size.

The composition of the nanoparticles was determined by atomic absorption spectroscopy (AAS). The experimental data are shown in Table 1. The experimental molar ratios of silver and gold agree well with the expected values.

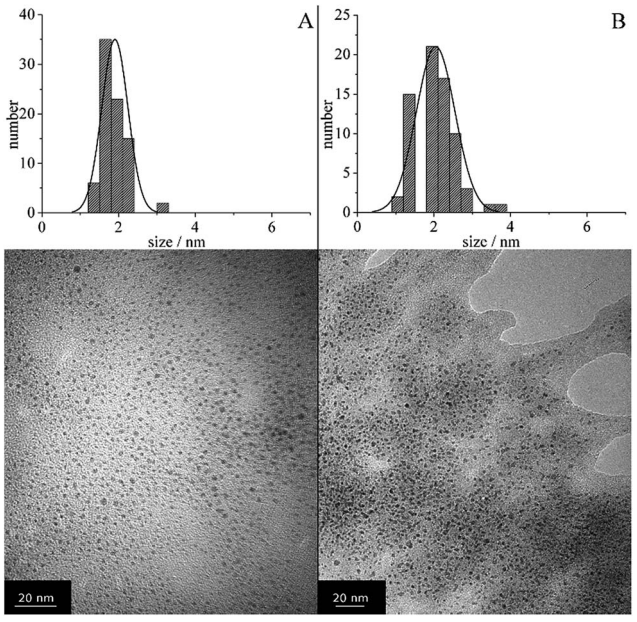

Fig. 1 Transmission electron micrograph of Ag : Au 30 : 70 nanoparticles (A) and Ag : Au 20 : 80 nanoparticles (B).

The stability against agglomeration depends on the pH of the dispersion and the protonation equilibrium of the terminal carboxylic acid groups of the ligand. We used a borate/hydrochloric acid buffer to keep the pH at 9. Borate was chosen because it is also generated during the reduction with sodium borohydride, thus avoiding additional chemical components in the system. The deprotonated carboxylic acid led to high electrostatic stability, even in the presence of a high electrolyte concentration (a final buffer concentration of 20 mM tetraborate).

Although the nanoparticles were too small to conduct reliable dynamic light scattering measurements, it can be safely assumed that the nanoparticles possess a negative zeta potential and a point of zero charge similar to the pK_a of 11-MUA. This was reported to be 5.4 for a monolayer of 11-MUA on a gold surface.[45] We can conclude that at a pH below 5, the carboxylic group will be mostly protonated, and agglomeration will occur.

The colour of the purified and concentrated dispersions ranged from colourless (high Au content) to light brown (high Ag content) under visible light. Pure gold nanoparticles and samples with a molar Ag : Au composition between 10 : 90 and 60 : 40 exhibited good visible fluorescence under a 254/365 nm fluorescence lamp. Nanoparticles with a higher silver content than 60 mol% and pure silver nanoparticles did not show autofluorescence. This can most likely be attributed to the slightly larger particle size, as silver clusters were reported to show autofluorescence only at diameters of 1.3 nm and below.[29,30] The colour of the emitted fluorescence ranged from bright orange (high Au content) to red (high Ag content). To investigate the optical properties of the samples further, we used fluorescence spectroscopy. The absorption spectra of the nanoparticles were almost symmetric and had absorption maxima at wavelengths between 250 nm and 330 nm, although no clear trend was visible (Fig. 3). The symmetric emission spectra showed a large Stokes shift of up to 360 nm (Ag : Au 20 : 80), consistent with previous reports.[25,41] The large shifts which are similar to those in luminescent Au(I) complexes can be attributed to electronic d–sp electronic transitions.[46,47] The maximum emission wavelength showed a redshift with a clear trend from 608 nm (Ag : Au 10 : 90) to 645 nm (Ag : Au 60 : 40). Interestingly, this red shift of the maximum absorption wavelength was increasing with increasing silver content, consistent with the results reported for other silver–gold nanoparticles.[40] For pure gold nanoparticles (1.5 nm), we measured an absorption maximum at 320 nm and an emission maximum at 607 nm.

The fluorescence of the nanoparticles remained visible when the particles were precipitated and freeze-dried, indicating a high stability of the noble metal–sulphur bond. The emission spectra of the nanoparticles only changed slightly in intensity when the dispersions were irradiated at different wavelengths (Fig. 4). Neither the maximum excitation wavelength nor the maximum emission wavelength shifted significantly, proving that the detected signal is indeed fluorescence and not just scattered light.

Table 1 Experimental molar compositions of nanoparticles, as measured by AAS, and the particle diameter, as measured by DCS. The DCS results represent the maxima of the particle size distribution

Theoretical composition Ag : Au in mol%	0 : 100	10 : 90	20 : 80	30 : 70	40 : 60	50 : 50	60 : 40	70 : 30	80 : 20	90 : 10	100 : 0
Experimental composition Ag : Au in mol%	0 : 100	12 : 88	20 : 80	28 : 72	40 : 60	50 : 50	63 : 37	68 : 32	79 : 21	93 : 7	100 : 0
Diameter (DCS) in nm	1.5	1.7	1.8	1.8	1.8	1.8	2.1	2.0	2.1	2.1	2.2

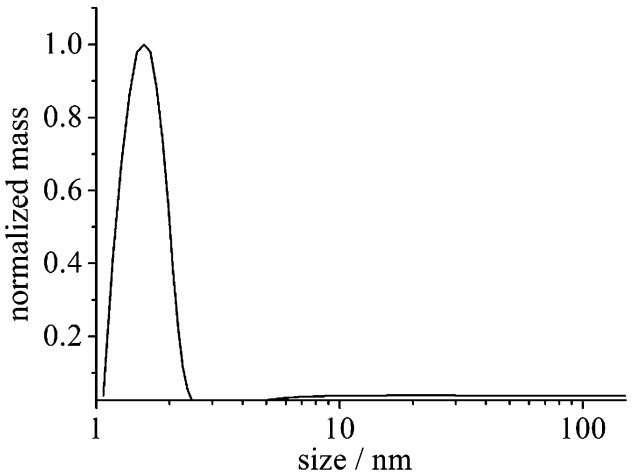

Fig. 2 Disc centrifugal sedimentation of Ag : Au 10 : 90 nanoparticles.

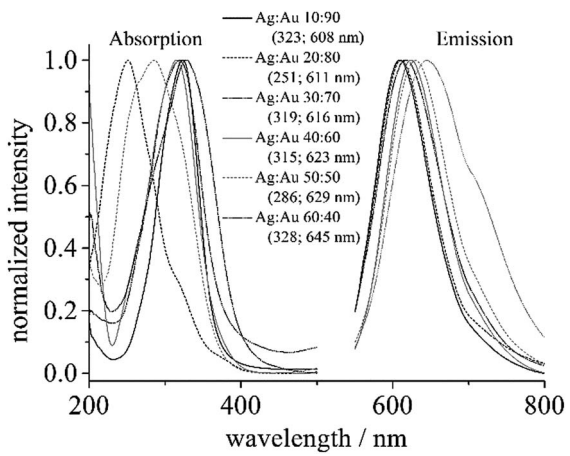

Fig. 3 Excitation and emission spectra of nanoparticles with different molar Ag : Au compositions. The numbers in parentheses indicate the maxima of the absorption and emission bands, respectively, for the six samples.

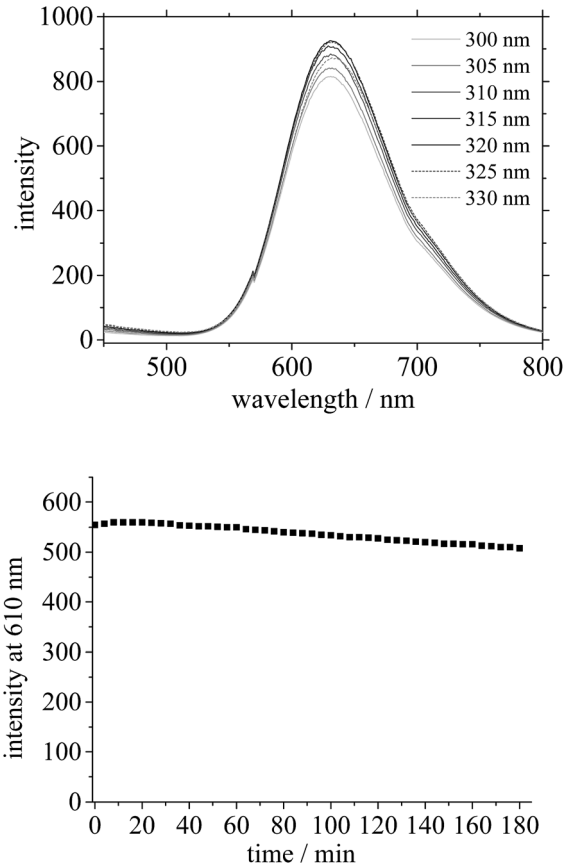

Fig. 4 Emission spectra of Ag : Au 40 : 60 nanoparticles at different excitation wavelengths (top) and fluorescence intensity of Ag : Au 10 : 90 nanoparticles at 610 nm recorded every 4 minutes during 180 minutes of irradiation (bottom).

The photostability of the nanoparticles was studied for the Ag : Au 10 : 90 samples in a permanent irradiation experiment. The nanoparticle dispersion was continuously irradiated inside a fluorescence spectrometer with a Xenon flash lamp at 300 nm for 180 min. Every 8 min, an emission spectrum was recorded. The fluorescence intensity at 610 nm showed only a slow decay over time from an intensity of 555 units at the first measurement to 507 units after 180 min (Fig. 4). This decrease in intensity of just about 9% demonstrates the excellent stability of the nanoparticles towards photobleaching. The experiment was only carried out for the Ag : Au 10 : 90 samples, but we do not expect a significant difference for the samples with another composition due to their structural similarity (alloyed metallic nanoparticles).

IR-spectroscopy and ^{1}H-NMR spectroscopy can be used to further assess the properties of nanoparticles, *e.g.* ligand orientation.[34,48–50] The orientation is an important factor if a bifunctional ligand is attached because the accessibility of specific functional groups is critical for a subsequent chemical modification of the particle surface. In IR-spectroscopy, the

disappearance of a characteristic group, in this case the S–H and COOH bands, can be interpreted as evidence for a bond from the ligand to the particle surface through this specific functionality.

Three representative FTIR-spectra are shown in Fig. 5. The free ligand shows distinctive bands at 2915/2848 cm^{-1} (symmetric and asymmetric $-CH_2-$ stretching), 2550 cm^{-1} (S–H stretching), 1690 cm^{-1} (C═O stretching), 1290–1188 cm^{-1} ($-CH_2-$ progression bands) and 933 cm^{-1} (out-of-plane OH bend), an indication of hydrogen bridging from the formation of carboxylic acid dimers. Purified, buffered (pH 9) and freeze-dried Au : Ag 50 : 50 nanoparticles show sharp $-CH_2-$ bands at 2916/2847 cm^{-1} and weak progression bands at 1297–1209 cm^{-1} which indicate an ordered all-trans structure of the aliphatic chain of the ligand.[51,52] The absence of the S–H band ($\sim$2550 cm^{-1}) indicates that the mercaptoundecanoic acid is bound to the metal by the thiol group. A shift of the C═O absorption to 1564 cm^{-1} indicates a deprotonated carboxylate group, consistent with the precipitation of the sample at pH 9.

The third spectrum was recorded from Au : Ag 50 : 50 particles that were precipitated from dispersion with hydrochloric acid, *i.e.* at low pH. Here we see characteristic bands of $-CH_2-$ at 2916/2847 cm^{-1}, weak progression bands at 1294–1195 cm^{-1}, and again a missing S–H band. The C═O stretching at 1699 cm^{-1} indicates the presence of the protonated terminal carboxylic acid.

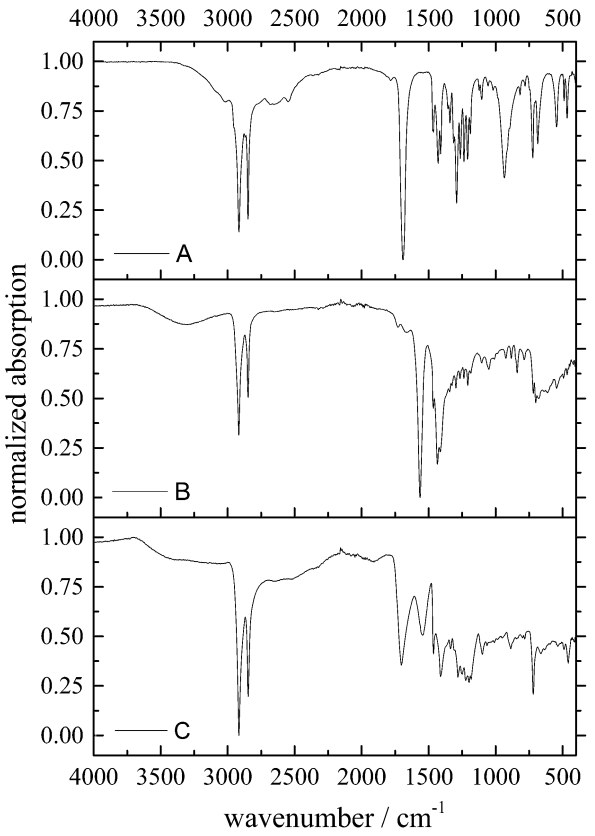

Fig. 5 Infrared spectroscopy of A: 11-MUA, B: freeze-dried Ag : Au 50 : 50 nanoparticles, precipitated from the buffered suspension, and C: freeze-dried Ag : Au 50 : 50 nanoparticles from acidic precipitation.

^{1}H-NMR spectroscopy was used to obtain further information about the ligand orientation on the particle surface because the interaction of a ligand with a nanoparticle surface leads to distinct changes in the resulting spectrum compared to the dissolved ligand molecules. Adsorbed (chemisorbed) molecules show peak broadening and a different chemical shift. The broadening is a result of fast spin relaxation from dipolar interactions with the metallic core and increases with proximity of the methylene groups to the nanoparticle surface. Furthermore, a change in magnetic susceptibility at ligand–metal boundary and spin–spin relaxation broadening which depends on the velocity of the nanoparticles in solution may contribute to a significant difference between the free ligand and adsorbed species, up to a complete disappearance of the peaks of the methylene groups that are closest to the nanoparticle. This allows the identification of terminal and particle-facing groups and thus permits the assessment of the ligand orientation.[34,49,53–55]

In Fig. 6, the ^{1}H-NMR spectra of pure 11-MUA (300 MHz, D_2O, 25 μL NaOD, $\delta = 1.28$ (m, 12H, CH_2), $\delta = 1.53$ (m, 4H, CH_2), $\delta = 2.16$ (t, 2H, CH_2–COO^-), $\delta = 2.49$ ppm (t, 2H, CH_2–S^-)), and of purified Ag : Au 70 : 30 nanoparticles (300 MHz, D_2O, 25 μL NaOD, $\delta = 1.0$–1.48 (br m, 12H, CH_2), $\delta = 1.48$–1.85 (br m, 4H, CH_2), $\delta = 2.10$–2.42 (br m, t, 2H, CH_2–COO^-)) are shown. In comparison with dissolved 11-MUA, the peaks of the functionalized nanoparticles are strongly broadened and no free ligand is present. Obviously, the α-methylene protons next to the thiol group (4) have disappeared. This indicates that the ligand is bound to the particle surface with the thiol group, leaving the terminal carboxylic acid exposed for stability manipulation through pH-changes and possible modification of the particles *via* coupling reactions. In the ligand spectrum, a small triplet at

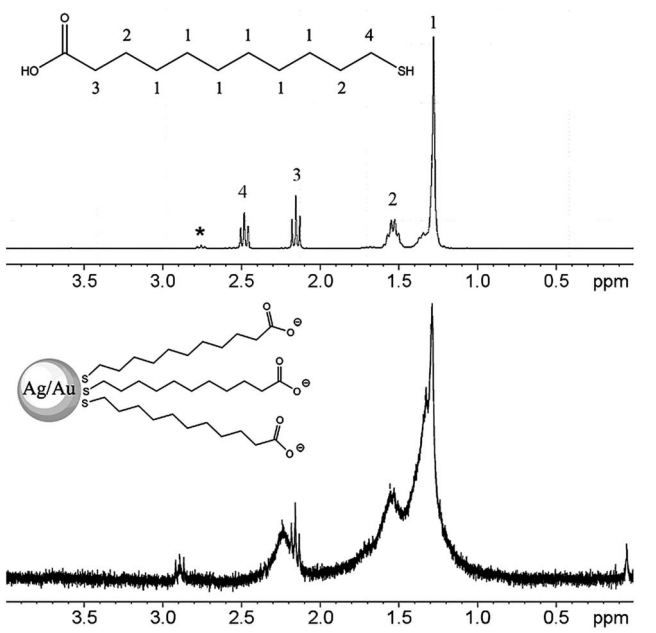

Fig. 6 Representative ^{1}H-NMR of 11-MUA (top) and purified Ag : Au 70 : 30 nanoparticles, functionalized with 11-MUA (bottom).

2.76 ppm (*) is visible which originates from the α-methylene group of the disulphide-form of the ligand.[49] In the spectrum of the nanoparticles, this triplet is found at 2.90 ppm. The triplet in the spectrum of the nanoparticles, visible overlapping with a broad peak at 2.16 ppm, can be attributed to the methylene group next to the carboxylate (3). The signal is the least broadened, because of its maximum distance to the metal surface. The overlapping broadened peak, however, indicates that the ligand shell is not completely oriented with the thiol-groups towards the gold but with some carboxylate groups located in proximity to the nanoparticle surface as well.

The cytotoxicity of the alloyed silver–gold nanoparticles was analysed by the MTT assay (Fig. 7). For a better comparison between the samples, the total metal concentrations of 5 μg mL^{-1} (5 ppm) and 50 μg mL^{-1} (50 ppm) were used. The calculated nanoparticle concentrations for the different particle samples, based on the average diameter in DCS and the AAS values for silver and gold, are given in Table 2. Previously, we had reported that tris(3-sulfonatophenyl)phosphine- or poly(*N*-vinylpyrrolidone)-stabilized gold nanoparticles with a diameter of 5 nm were not toxic for hMSCs after 24 h at 5–20 μg mL^{-1}.[38] Here we found a decrease of the cell viability after 24 h incubation with 50 μg mL^{-1} of 11-MUA-stabilized small gold nanoparticles (Fig. 7A). Small gold nanoparticles (diameter 1.4 nm) were shown previously to be more cytotoxic than smaller or larger ones.[56,57]

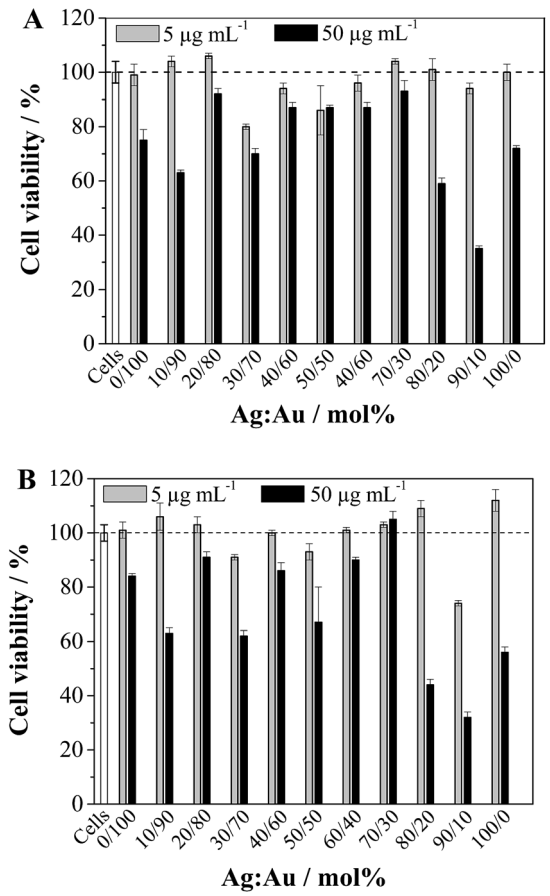

Fig. 7 MTT assays of HeLa cells after incubation with different concentrations of alloyed silver–gold nanoparticles for 24 h (A) and 72 h (B).

Pure silver nanoparticles displayed no toxic effect for HeLa cells after 24 h and 72 h at a metal concentration of 5 μg mL^{-1}. With increasing concentration of silver nanoparticles (50 μg mL^{-1}), the cell viability rapidly decreased, as expected for the cytotoxic silver ion.[58] Biological studies on ligand-free gold–silver nanoalloys were reported by Barcikowski *et al.* They found an increasing cytotoxicity with increasing silver content and ascribed this effect to released silver ions, possibly enhanced by the presence of the noble metal gold, forming a local electrochemical element with silver.[39,44]

Interestingly, the increase of the dose of silver in alloyed silver–gold nanoparticles did not lead to a monotonous decrease of cell viability. In particular, the Ag : Au 90 : 10 nanoparticles were more toxic than pure silver nanoparticles (100 : 0). This is an unexpected result that cannot be explained so far and deserves further attention. However, we have found that this discontinuity was reproducible. Barcikowski *et al.* reported similar observations with alloyed silver–gold nanoparticles from laser ablation in mammalian gametes.[39]

Uptake studies were performed on HeLa cells with two types of silver–gold nanoparticles, *i.e.* Ag : Au 30 : 70 and Ag : Au 50 : 50 nanoparticles in serum-free medium for 5 h. To avoid the interaction of the nanoparticles with serum proteins that may act as a protective layer, shielding the nanoparticle surface from interactions with the cells,[29,59–61] the cellular uptake studies were performed in the absence of proteins. In Fig. 8, it is clearly visible that the bimetallic nanoparticles are mostly localized on the cell membrane. Due to the very small size of investigated nanoparticles, a diffuse nature of fluorescence was observed. To shed further light on the effect of protein adsorption on the nanoparticle surface, the cellular uptake of silver–gold nanoparticles was investigated in serum-supplemented medium.

The uptake studies in serum-supplemented medium showed a less pronounced localization of the nanoparticles around the cell membrane compared with the cellular uptake in serum-free medium after 5 h (Fig. 9). Shang *et al.* showed a reduced amount of internalized silver nanoparticles in the presence of proteins.[29] This observation can be explained by the better stability of the nanoparticles in protein-containing medium.[62] In general, the uptake and the cytotoxicity of small metallic nanoparticles depend on their size[44] and their surface functionalization.[47] In this case, the uptake mechanism is not known, but it is likely that cellular uptake occurs by endocytosis as observed for nanoparticles in general[63–65] and small gold nanoparticles in HeLa cells in particular.[66] Recent studies have also demonstrated a size-dependent toxicity of gold nanoparticles.[67,68] The ligand chemistry may also affect the cytotoxicity of gold nanoclusters.[57] Polavarapu *et al.* demonstrated a rather low toxicity of glutathione-capped gold clusters towards human neuroblastoma cells even at very high concentrations (400 μg mL^{-1}).[69]

The incubation of HeLa cells with Ag : Au 30 : 70 nanoparticles and Ag : Au 50 : 50 nanoparticles for 24 h in serum-supplemented medium clearly showed the red fluorescing

Table 2 Calculated nanoparticle concentrations for cell viability experiments, expressed as nmol of nanoparticles per mL

Theoretical composition Ag : Au in mol%	0 : 100	10 : 90	20 : 80	30 : 70	40 : 60	50 : 50	60 : 40	70 : 30	80 : 20	90 : 10	100 : 0
Nanoparticle concentration at 5 μg mL^{-1} metal in nmol mL^{-1}	0.24	0.17	0.15	0.15	0.16	0.17	0.11	0.14	0.13	0.14	0.14
Nanoparticle concentration at 50 μg mL^{-1} metal in nmol mL^{-1}	2.43	1.72	1.49	1.54	1.61	1.68	1.11	1.38	1.29	1.43	1.42

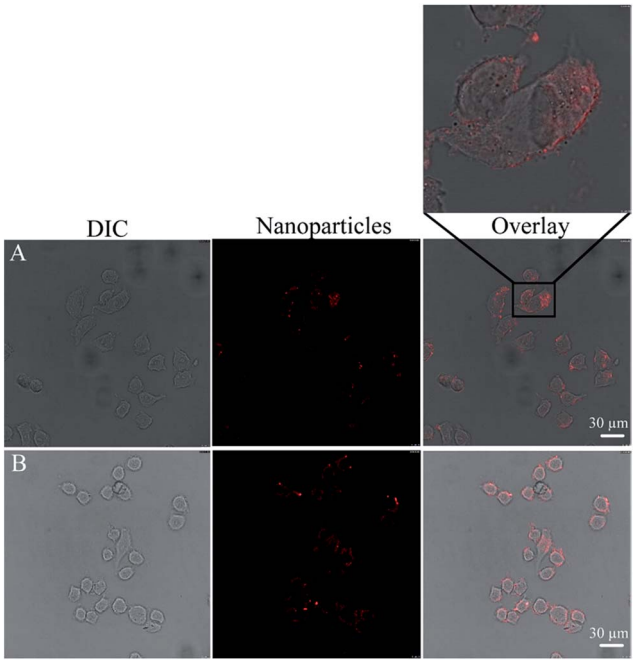

Fig. 8 CLSM images of HeLa cells after incubation with Ag : Au 30 : 70 (A) and Ag : Au 50 : 50 (B) nanoparticles for 5 h in serum-free cell culture medium. DIC: differential interference contrast. The nanoparticles have a red colour.

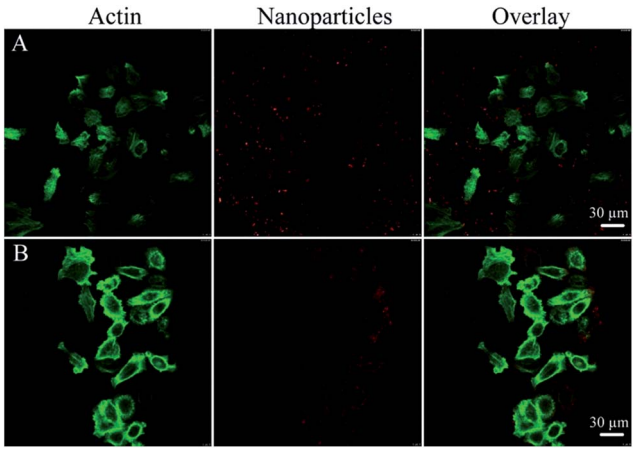

Fig. 9 CLSM images of HeLa cells after incubation with Ag : Au 30 : 70 (A) and Ag : Au 50 : 50 (B) nanoparticles for 5 h in serum-supplemented medium. The nanoparticles have a red colour and the cell cytoskeleton (actin) is stained green.

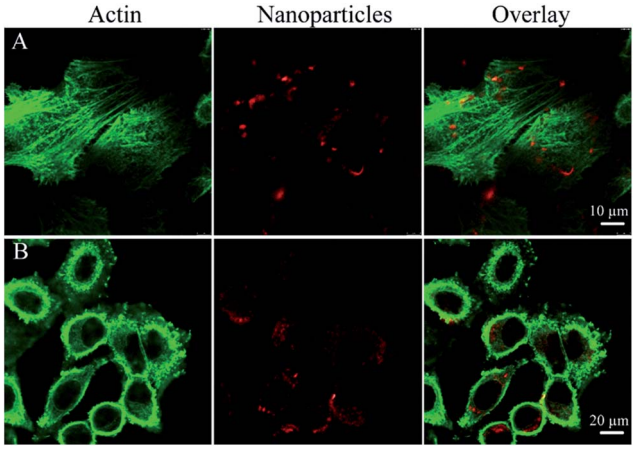

Fig. 10 CLSM images of HeLa cells after incubation with Ag : Au 30 : 70 (A) and Ag : Au 50 : 50 (B) nanoparticles for 24 h in serum-supplemented medium. The nanoparticles have a red colour and the cell cytoskeleton (actin) is stained green.

particles in the cytoplasm (Fig. 10) around the nucleus, indicating the successful internalization of bimetallic nanoparticles in the cells. The red fluorescent dots within the cells are not individual nanoparticles but a number of accumulated nanoparticles in endosomal vesicles.[66,70]

Note that these results were obtained with one cell line (HeLa) and cannot be quantitatively transposed to other cell lines. This is due to the variability of cell lines towards particles, as it was summarized for silver.[58] However, the general trends should hold for other cell lines as well.

Conclusions

Ultra-small bimetallic silver gold nanoparticles were prepared with nine different compositions. The presented wet-chemical synthesis is an easy way to generate purified ultra-small silver–gold nanoparticles with variable molar ratios of silver and gold that show fluorescence for molar compositions Ag : Au between 60 : 40 and 10 : 90. The ligand 11-MUA is bound to the particle surface by the thiol group that permits further possible functionalization at the terminal carboxylate group. The nanoparticles are taken up by HeLa cells after 24 h incubation and do not exert toxicity towards the cells at 5 μg mL^{-1} (5 ppm). Even at 50 μg mL^{-1} (50 ppm), the cell viability remained well above 50%, except for a high silver content. The autofluorescence intensity of the nanoparticles is high enough to follow their uptake by cells with confocal laser scanning microscopy without

any additional fluorophore. Taking this into account, the synthesized nanoparticles represent a suitable probe for cellular imaging with variable ratios of silver and gold.

Acknowledgements

We thank the Deutsche Forschungsgemeinschaft (DFG) for financial support of this project within the Priority Program NanoBioResponses (SPP 1313). We thank Prof. Shirley Knauer, University of Duisburg-Essen, for access to the confocal laser scanning microscope.

Notes and references

1 G. Schmid, *Nanoparticles. From Theory to Application*, Wiley-VCH, Weinheim, 2004.
2 A. Leifert, Y. Pan-Bartnek, U. Simon and W. Jahnen-Dechent, *Nanoscale*, 2013, **5**, 6224–6242.
3 E. C. Dreaden, A. M. Alkilany, X. Huang, C. J. Murphy and M. A. El-Sayed, *Chem. Soc. Rev.*, 2012, **41**, 2740–2779.
4 S. Barcikowski and F. Mafune, *J. Phys. Chem. C*, 2011, **115**, 4985.
5 M. Brust and C. J. Kiely, *Coll. Surf. A: Physicochem. Eng. Aspects*, 2002, **202**, 175–186.
6 M. Homberger and U. Simon, *Philos. Trans. R. Soc., A*, 2010, **368**, 1405–1453.
7 P. K. Jain, X. Huang, I. H. El-Sayed and M. A. El-Sayed, *Acc. Chem. Res.*, 2008, **41**, 1578–1586.
8 R. A. Sperling, P. Rivera, F. Zhang, M. Zanella and W. J. Parak, *Chem. Soc. Rev.*, 2008, **37**, 1896–1908.
9 V. Voliani, G. Signore, O. Vittorio, P. Faraci, S. Luin, J. Perez-Prieto and F. Beltram, *J. Mater. Chem. B*, 2013, **1**, 4225–4230.
10 K. Loza, J. Diendorf, C. Greulich, L. Ruiz-Gonzales, J. M. Gonzalez-Calbet, M. Vallet-Regi, M. Koeller and M. Epple, *J. Mater. Chem. B*, 2014, **2**, 1634–1643.
11 K. Loza, C. Sengstock, S. Chernousova, M. Koeller and M. Epple, *RSC Adv.*, 2014, **4**, 35290–35297.
12 S. Banerjee, K. Loza, W. Meyer-Zaika, O. Prymak and M. Epple, *Chem. Mater.*, 2014, **26**, 951–957.
13 S. Agnihotri, S. Mukherji and S. Mukherji, *RSC Adv.*, 2014, **4**, 3974–3983.
14 C. C. Huang, Z. Yang, K. H. Lee and H. T. Chang, *Angew. Chem., Int. Ed.*, 2007, **46**, 6824–6828.
15 C. A. J. Lin, C. H. Lee, J. T. Hsieh, H. H. Wang, J. K. Li, J. L. Shen, W. H. Chan, H. I. Yeh and W. H. Chang, *J. Med. Biol. Eng.*, 2009, **29**, 276–283.
16 L. Shang, S. J. Dong and G. U. Nienhaus, *Nano Today*, 2011, **6**, 401–418.
17 Y. C. Shiang, C. C. Huang, W. Y. Chen, P. C. Chen and H. T. Chang, *J. Mater. Chem.*, 2012, **22**, 12972–12982.
18 Y. Lu and W. Chen, *Chem. Soc. Rev.*, 2012, **41**, 3594–3623.
19 J. Zheng, P. R. Nicovich and R. M. Dickson, *Annu. Rev. Phys. Chem.*, 2007, **58**, 409–431.
20 C. Guo and J. Irudayaraj, *Anal. Chem.*, 2011, **83**, 2883–2889.
21 H. Wei, Z. Wang, L. Yang, S. Tian, C. Hou and Y. Lu, *Analyst*, 2010, **135**, 1406–1410.
22 L. Shang, F. Stockmar, N. Azadfar and G. U. Nienhaus, *Angew. Chem., Int. Ed.*, 2013, **52**, 11154–11157.
23 S. Palmal, S. K. Basiruddin, A. R. Maity, S. C. Ray and N. R. Jana, *Chem.–Eur. J.*, 2013, **19**, 943–949.
24 L. Shang, N. Azadfar, F. Stockmar, W. Send, V. Trouillet, M. Bruns, D. Gerthsen and G. U. Nienhaus, *Small*, 2011, **7**, 2614–2620.
25 J. Sun, J. Zhang and Y. Jin, *J. Mater. Chem. C*, 2013, **1**, 138–143.
26 Z. Zhang, L. Xu, H. Li and J. Kong, *RSC Adv.*, 2012, **3**, 59–63.
27 J. L. Li, X. Q. An and Y. Y. Zhu, *J. Nanopart. Res.*, 2012, **14**, 1325.
28 B. Sengupta, C. M. Ritchie, J. G. Buckman, K. R. Johnsen, P. M. Goodwin and J. T. Petty, *J. Phys. Chem. C*, 2008, **112**, 18776–18782.
29 L. Shang, R. M. Dörlich, V. Trouillet, M. Bruns and G. U. Nienhaus, *Nano Res.*, 2012, **5**, 531–542.
30 H. Xu and K. S. Suslick, *ACS Nano*, 2010, **4**, 3209–3214.
31 X. Le Guével, B. Hötzer, G. Jung, K. Hollemeyer, V. Trouillet and M. Schneider, *J. Phys. Chem. C*, 2011, **115**, 10955–10963.
32 H. Liu, X. Zhang, X. Wu, L. Jiang, C. Burda and J. J. Zhu, *Chem. Commun.*, 2011, **47**, 4237–4239.
33 J. Xie, Y. Zheng and J. Y. Ying, *J. Am. Chem. Soc.*, 2009, **131**, 888–889.
34 M. Cargnello, N. L. Wieder, P. Canton, T. Montini, G. Giambastiani, A. Benedetti, R. J. Gorte and P. Fornasiero, *Chem. Mater.*, 2011, **23**, 3961–3969.
35 Y. Guo, Z. L. Wang, H. Shao and X. Jiang, *Analyst*, 2011, **137**, 301–304.
36 S. K. Tripathy and Y. T. Yu, *Spectrochim. Acta, Part A*, 2009, **72**, 841–844.
37 S. Link, Z. L. Wang and M. A. El-Sayed, *J. Phys. Chem. B*, 1999, **103**, 3529–3533.
38 D. Mahl, J. Diendorf, S. Ristig, C. Greulich, Z. A. Li, M. Farle, M. Koeller and M. Epple, *J. Nanopart. Res.*, 2012, **14**, 1153.
39 D. Tiedemann, U. Taylor, C. Rehbock, J. Jakobi, S. Klein, W. A. Kues, S. Barcikowski and D. Rath, *Analyst*, 2014, **139**, 931–942.
40 X. Le Guével, V. Trouillet, C. Spies, K. Li, T. Laaksonen, D. Auerbach, G. Jung and M. Schneider, *Nanoscale*, 2012, **4**, 7624.
41 T. Y. Zhou, L. P. Lin, M. C. Rong, Y. Q. Jiang and X. Chen, *Anal. Chem.*, 2013, **85**, 9839–9844.
42 M. Ganguly, A. Pal, Y. Negishi and T. Pal, *Langmuir*, 2013, **29**, 2033–2043.
43 T. Udayabhaskararao, Y. Sun, N. Goswami, S. K. Pal, K. Balasubramanian and T. Pradeep, *Angew. Chem., Int. Ed.*, 2012, **51**, 2155–2159.
44 S. Grade, J. Eberhard, J. Jakobi, A. Winkel, M. Stiesch and S. Barcikowski, *Gold Bull.*, 2014, **47**, 83–93.
45 J. F. Smalley, K. Chalfant, S. W. Feldberg, T. M. Nahir and E. F. Bowden, *J. Phys. Chem. B*, 1999, **103**, 1676–1685.
46 Y. A. Lee and R. Eisenberg, *J. Am. Chem. Soc.*, 2003, **125**, 7778–7779.
47 Z. Wu and R. Jin, *Nano Lett.*, 2010, **10**, 2568–2573.
48 M. Brust, M. Walker, D. Bethell, D. J. Schiffrin and R. Whyman, *Chem. Commun.*, 1994, 801–802.

49 D. Gentili, G. Ori and M. Comes, *Chem. Commun.*, 2009, 5874–5876.
50 E. Reyes, R. Madueño, M. Blázquez and T. Pineda, *J. Phys. Chem. C*, 2010, **114**, 15955–15962.
51 K. S. Birdi, *Self-assembly Monolayer Structures of Lipids and Macromolecules at Interfaces*, Springer US, Boston, MA, 2002.
52 M. J. Hostetler, S. J. Green, J. J. Stokes and R. W. Murray, *J. Am. Chem. Soc.*, 1996, 4212–4213.
53 M. J. Hostetler, J. E. Wingate, C. J. Zhong, J. E. Harris, R. W. Vachet, M. R. Clark, J. D. Londono, S. J. Green, J. J. Stokes, G. D. Wignall, G. L. Glish, M. D. Porter, N. D. Evans and R. W. Murray, *Langmuir*, 1998, **14**, 17–30.
54 J. S. Seo, D. M. Son, H. Lee, J. Kim and Y. Kim, *Bull. Korean Chem. Soc.*, 2009, **30**, 2651–2654.
55 R. H. Terrill, T. A. Postlethwaite, C. H. Chen, C. D. Poon, A. Terzis, A. Chen, J. E. Hutchison, M. R. Clark and G. Wignall, *J. Am. Chem. Soc.*, 1995, **117**, 12537–12548.
56 M. Semmler-Behnke, W. G. Kreyling, J. Lipka, S. Fertsch, A. Wenk, S. Takenaka, G. Schmid and W. Brandau, *Small*, 2008, **4**, 2108–2111.
57 Y. Pan, A. Leifert, D. Ruau, S. Neuss, J. Bornemann, G. Schmid, W. Brandau, U. Simon and W. Jahnen-Dechent, *Small*, 2009, **5**, 2067–2076.
58 S. Chernousova and M. Epple, *Angew. Chem., Int. Ed.*, 2013, **52**, 1636–1653.
59 E. Caballero-Díaz, C. Pfeiffer, L. Kastl, P. Rivera-Gil, B. Simonet, M. Valcárcel, J. Jiménez-Lamana, F. Laborda and W. J. Parak, *Part. Part. Syst. Charact.*, 2013, **30**, 1079–1085.
60 L. Shang and G. U. Nienhaus, *Mater. Today*, 2013, **16**, 58–66.
61 D. Walczyk, F. B. Bombelli, M. P. Monopoli, I. Lynch and K. A. Dawson, *J. Am. Chem. Soc.*, 2010, **132**, 5761–5768.
62 S. Kittler, C. Greulich, J. S. Gebauer, J. Diendorf, L. Treuel, L. Ruiz, J. M. Gonzalez-Calbet, M. Vallet-Regi, R. Zellner, M. Köller and M. Epple, *J. Mater. Chem.*, 2010, **20**, 512–518.
63 I. Canton and G. Battaglia, *Chem. Soc. Rev.*, 2012, **41**, 2718–2739.
64 T. G. Iversen, T. Skotland and K. Sandvig, *Nano Today*, 2011, **6**, 176–185.
65 G. Sahay, D. Y. Alakhova and A. V. Kabanov, *J. Controlled Release*, 2010, **145**, 182–195.
66 L. Yang, L. Shang and G. U. Nienhaus, *Nanoscale*, 2013, **5**, 1537–1543.
67 Y. Pan, S. Neuss, A. Leifert, M. Fischler, F. Wen, U. Simon, G. Schmid, W. Brandau and W. Jahnen-Dechent, *Small*, 2007, **3**, 1941–1949.
68 W. G. Kreyling, S. Hirn, W. Möller, C. Schleh, A. Wenk, G. Celik, J. Lipka, M. Schäffler, N. Haberl, B. D. Johnston, R. Sperling, G. Schmid, U. Simon, W. J. Parak and M. Semmler-Behnke, *ACS Nano*, 2013, **8**, 222–233.
69 L. Polavarapu, M. Manna and Q. H. Xu, *Nanoscale*, 2011, **3**, 429–434.
70 X. Jiang, C. Rücker, M. Hafner, S. Brandholt, R. M. Dörlich and G. U. Nienhaus, *ACS Nano*, 2010, **4**, 6787–6797.